PAPER

Facile formation and redox of benzoxazole-2-thiolate-bridged dinuclear Pt(II/III) complexes†

Zhe Wang,[a] Lu Jiang,[a] Zhi-Pan Liu,[b] C. R. Raymond Gan,[a] Zhaolin Liu,[c] Xin-Hai Zhang,[c] Jin Zhao*[a,c] and T. S. Andy Hor*[a,c]

Reaction of [Pt(L)(μ-Cl)]$_2$ (L = ppy (2-phenylpyridine) or bzq (benzo[*h*]quinoline)) with 2-mercaptobenzoxazole (NOSH) and NaOAc in THF at r.t. yields the dinuclear Pt(II) d^8–d^8 complexes [Pt$_2$L$_2$(μ-NOS-κN,S)$_2$] (L = ppy, **1**; L = bzq, **2**) and the Pt(III) d^7–d^7 complexes [Pt$_2$(ppy)$_2$(μ-NOS-κN,S)$_2$(NOS-κS)$_2$] (L = ppy, **3**; L = bzq, **4**) in one pot. The C,N-cyclometalated ligand is chelating whereas the N,S-donating benzoxazole-2-thiolates doubly bridge the two metal centers. The Pt⋯Pt separations of 3.0204(3) and 2.9726(8) Å in **1** and **2** contract to 2.685(1) Å in **3** and 2.6923(3) Å in **4**, respectively, when two S-bound thiolate ligands coordinate *trans*- to the Pt⋯Pt axis. However, cyclometalation is preserved and there is minimum perturbation of the bridging ligands. Complexes **3** and **4** can be also obtained by oxidative addition of the thiolate ligand. In the presence of NaBH$_4$, **3** and **4** can be reduced to **1** and **2**, respectively. At r.t., **1** and **2** exhibit intense orange-red luminescence at 625 nm and 631 nm, respectively. The electrochemical properties of **1**–**4** have been also discussed.

Introduction

Dinuclear Pt(II) complexes have attracted much research interest in their structural[1–3] and photoluminescent properties.[4–11] Many of their potential applications, such as detection of VOCs (volatile organic compounds)[12,13] and in light-emitting diodes (LEDs)[14–16] result from the MMLCT (metal–metal to ligand charge transfer) transition as the notable excited state in which the emission energy shows a strong dependence on the inter- or intramolecular Pt⋯Pt interactions.[17] For example, the VOC vapor-induced luminescent change in *syn*-[Pt(bpy)(μ-pyt-κN,S)]$_2$-[PF$_6$]$_2$ (bpy = 2,2′-bipyridine, pyt = pyridine-2-thiolate) is attributed to the change of intermolecular Pt⋯Pt interaction between solvated and desolvated complexes.[18] Recently, analogous dinuclear Pt(II)–thiolate diimines have also been reported to show a correlation between intermolecular Pt⋯Pt interaction and luminescent behavior.[19] Steric control of the intramolecular Pt⋯Pt interaction has been achieved in a series of

cyclometalated pyrazole-bridged dinuclear Pt(II) complexes,[17] and their application as phosphorescent emitters in organic LEDs has been reported.[14] Dinuclear Pt(II) complexes can undergo two-electron two-center oxidative addition to give Pt(III)–Pt(III) complexes.[1,11,20–26] The luminescence properties of some of these d^7–d^7 complexes have been explored.[20,24,27] Most recently, Sicilia *et al.* reported a Pt(II) dinuclear complex, [Pt$_2$(bzq)$_2$(μ-NSS-κN,S)$_2$] (bzq = benzo[*h*]quinoline, NSS = benzothiazole-2-thiolate) and the corresponding Pt(III) dinuclear complexes [Pt$_2$(bzq)$_2$(μ-NSS-κN,S)$_2$X$_2$] (X = Cl, Br, I).[28] The Pt(II) complex shows notable luminescence quantum yield with red emission.[28]

As part of our continuous interest in dinuclear Pt(II) chemistry[29–31] and luminescent metal complexes,[32–34] we herein report a one-pot synthesis of the new dinuclear Pt(II) and Pt(III) complexes, [Pt$_2$(ppy)$_2$(μ-NOS-κN,S)$_2$] (**1**), [Pt$_2$(bzq)$_2$(μ-NOS-κN,S)$_2$] (**2**), [Pt$_2$(ppy)$_2$(μ-NOS-κN,S)$_2$(NOS-κS)$_2$] (**3**) and [Pt$_2$(bzq)$_2$(μ-NOS-κN,S)$_2$(NOS-κS)$_2$] (**4**) (ppy = 2-phenylpyridine, bzq = benzo[*h*]quinoline, NOS = benzoxazole-2-thiolate) from [Pt(L)(μ-Cl)]$_2$ (L = ppy, bzq) and 2-mercaptobenzoxazole (NOSH) in the presence of NaOAc. Their electrochemical and photoluminescent properties have been included in the study.

Results and discussion

### Synthesis and characterization of complexes 1–4

Dinuclear Pt(II) complexes [Pt$_2$L$_2$(μ-NOS-κN,S)$_2$] (**1** and **2**) and Pt(III) complexes [Pt$_2$L$_2$(μ-NOS-κN,S)$_2$(NOS-κS)$_2$] (**3** and **4**) (L = ppy, **1** and **3**; L = bzq, **2** and **4**) were obtained by one-pot reaction between [Pt(L)(μ-Cl)]$_2$ and NOSH in a ratio of 1.0 : 4.2

[a]Department of Chemistry, National University of Singapore, 3 Science Drive 3, Singapore 117543, Singapore. E-mail: andyhor@nus.edu.sg, chmzhaoj@nus.edu.sg
[b]Department of Chemistry, MOE Key Laboratory for Computational Physical Sciences, Fudan University, Shanghai 200433, People's Republic of China
[c]Institute of Materials Research and Engineering, Agency for Science, Technology and Research, 3 Research Link, Singapore 117602, Singapore
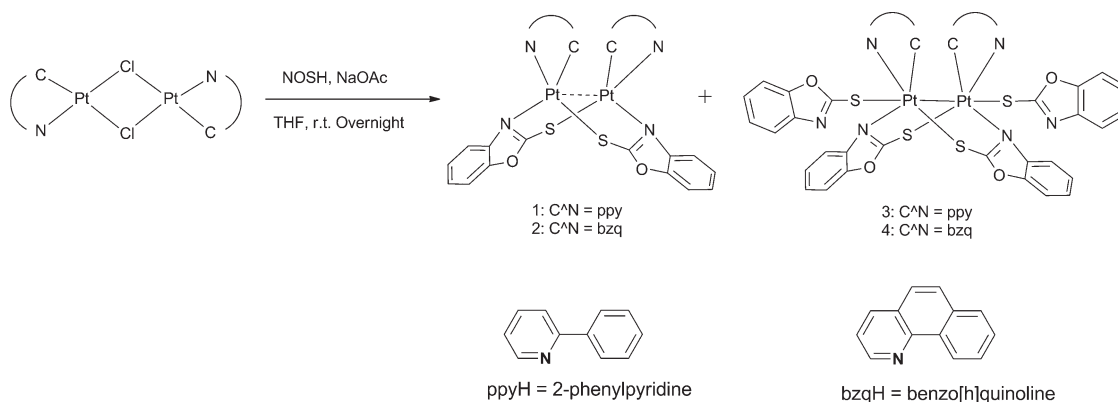
Scheme 1 Synthesis of complexes **1–4**.

in THF at r.t. in the presence of NaOAc (Scheme 1). The Pt(II) and Pt(III) complexes were separated by column chromatography. Complexes **1** and **2** were obtained as orange powder in yields of 35% and 32%, and **3** and **4** as red powder in yields of 23% and 17%, respectively. The ^{1}H, ^{13}C and ^{195}Pt NMR analysis of **1–4** only show one set of ligand resonances thus indicating that these complexes are present as symmetric isomers (*vide infra*). The ^{195}Pt NMR resonances of both **1** ($\delta = -3729$ ppm) and **2** ($\delta = -3730$ ppm) are significantly downfield-shifted when Pt(II) is oxidized to Pt(III) ($\delta = -2542$ ppm (**3**) and -2548 ppm (**4**)).

Complexes **3** and **4** can also be prepared through oxidative addition of 2.2 equivalents of NOSH in the presence of NaOAc at r.t in THF. In the presence of NaBH$_4$, **3** and **4** can be reduced to **1** and **2** under similar conditions.

Single-crystal X-ray crystallography analysis of **1** and **2** confirms the formation of dinuclear complexes. Both Pt(II) centers adopt a square planar geometry with two ppy or bzq ligands as chelating ligands and two NOS ligands doubly bridging two metals in a head to tail fashion (*anti*-isomer) (Fig. 1). The high *trans*-influence of cyclometalated carbon leads to the longer Pt–N$_{(N,S)}$ distances than the Pt–N$_{(CN)}$ ones in both **1** and **2**; a similar observation has been reported in other complexes with *anti*-configuration.[23,28,35] The intramolecular Pt···Pt separations are 3.0204(3) and 2.9726(8) Å for **1** and **2**, respectively (Table 1), which are similar to the non-bonding distances observed in other Pt(II)–Pt(II) complexes with two doubly bridged ligands,[9,11,18,19,36–38] such as 3.003(4) Å in *syn*-[Pt$_2$(d-*t*-bpy)$_2$(μ-NOS-κN,S)$_2$][ClO$_4$]$_2$ (d-*t*-bpy = 4,4′-di-*tert*-butyl-2,2′-bipyridine)[19] and 2.997(1) Å in *anti*-[Pt$_2$(bpy)$_2$(μ-pyt-κN,S)$_2$]-[PF$_6$]$_2$ (bpy = 2,2′-bipyridine, pyt = pyridine-2-thiolate).[18] In **2**, two bzq ligands are almost parallel to each other with dihedral angle of 6.81° (but not eclipsed) and with an interplanar space of 3.738 Å (defined as centroid to centroid distance of two bzq ligands), which are indicative of significant π–π interaction. However, in **1**, no π–π interaction is observed between two ppy ligands. This interaction could be attributed to the smaller Pt···Pt separation in **2** compared with **1**. It is interesting to note that despite the similar structure, complex **2** has a significantly larger Pt···Pt separation than [Pt$_2$(bzq)$_2$(μ-NSS-κN,S)$_2$][28] (Pt···Pt separation = 2.9101(8) Å). In both complexes, the Pt–N and Pt–S distances are very similar. The N···S bite distances (the distance between the two donor atoms of a ligand) of NOS and NSS are from 2.73 to 2.76 Å and 2.73–2.74 Å, respectively. The average
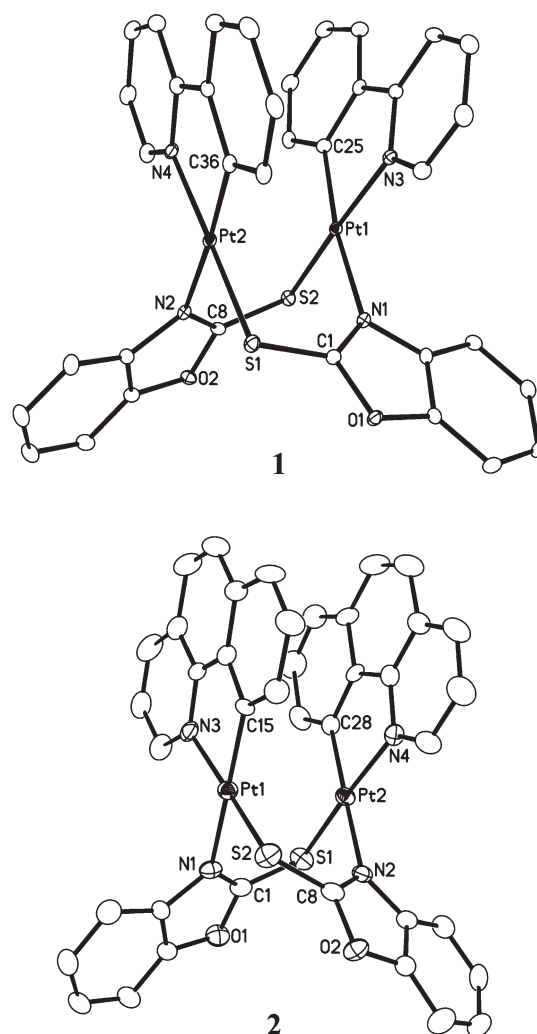

Fig. 1 ORTEP diagrams of **1** and **2** (30% probability ellipsoids). Solvent molecules and hydrogen atoms are omitted.

N–Pt–Pt–S torsion angle in **2** (16.3°) is slightly smaller than that in [Pt$_2$(bzq)$_2$(μ-NSS-κN,S)$_2$].[28] (17.8°).

The X-ray structures of **3** and **4** reveal that the NOS thiolate ligand acts as both a bridging and terminal ligand (Fig. 2). A similar coordination mode has been found in [Pt$_2$(ppy)$_2$(μ-pyt-

Table 1 Selected bond lengths, distances (Å) and angles (°) for **1–4**

1	Pt(1)···Pt(2)	3.0204(3)	Pt(1)–C(25)	1.988(3)
	Pt(1)–N(1)	2.129(3)	Pt(1)–N(3)	2.043(3)
	Pt(1)–S(2)	2.2949(8)	Pt(2)–C(36)	1.985(3)
	Pt(2)–N(2)	2.126(3)	Pt(2)–N(4)	2.043(3)
	Pt(2)–S(1)	2.2933(8)	C(25)–Pt(1)–N(3)	81.1(1)
	C(25)–Pt(1)–N(1)	172.5(1)	N(3)–Pt(1)–N(1)	93.8(1)
	C(25)–Pt(1)–S(2)	94.59(9)	N(3)–Pt(1)–S(2)	172.59(7)
	N(1)–Pt(1)–S(2)	89.97(7)	C(36)–Pt(2)–N(4)	81.0(1)
	C(36)–Pt(2)–N(2)	176.5(1)	N(4)–Pt(2)–N(2)	96.4(1)
	C(36)–Pt(2)–S(1)	95.0(1)	N(4)–Pt(2)–S(1)	175.05(8)
	N(2)–Pt(2)–S(1)	87.60(7)		
2	Pt(1)···Pt(2)	2.9726(8)	Pt(1)–C(15)	2.010(7)
	Pt(1)–N(3)	2.073(7)	Pt(1)–N(1)	2.149(6)
	Pt(1)–S(2)	2.297(2)	Pt(2)–C(28)	2.000(8)
	Pt(2)–N(4)	2.056(7)	Pt(2)–N(2)	2.126(6)
	Pt(2)–S(1)	2.299(2)	C(15)–Pt(1)–N(3)	81.3(3)
	C(15)–Pt(1)–N(1)	175.1(3)	N(3)–Pt(1)–N(1)	94.4(3)
	C(15)–Pt(1)–S(2)	94.3(3)	N(3)–Pt(1)–S(2)	173.7(1)
	N(1)–Pt(1)–S(2)	90.1(1)	C(15)–Pt(1)–Pt(2)	96.2(2)
	C(28)–Pt(2)–N(4)	82.2(3)	C(28)–Pt(2)–N(2)	175.8(3)
	N(4)–Pt(2)–N(2)	94.2(2)	C(28)–Pt(2)–S(1)	95.3(2)
	N(4)–Pt(2)–S(1)	173.8(1)	N(2)–Pt(2)–S(1)	88.5(1)
3	Pt(1)–Pt(1A)	2.685(1)	Pt(1)–C(15)	2.011(8)
	Pt(1)–N(3)	2.087(7)	Pt(1A)–N(1)	2.151(7)
	Pt(1)–S(1)	2.351(2)	Pt(1)–S(2)	2.437(3)
	C(15)–Pt(1)–N(3)	80.4(3)	C(15)–Pt(1)–N(1A)	175.6(3)
	N(3)–Pt(1)–N(1A)	95.6(3)	C(15)–Pt(1)–S(1)	97.4(3)
	N(3)–Pt(1)–S(1)	176.9(1)	N(1A)–Pt(1)–S(1)	86.7(1)
	C(15)–Pt(1)–S(2)	83.1(3)	N(3)–Pt(1)–S(2)	88.1(1)
	N(1A)–Pt(1)–S(2)	98.7(1)	S(1)–Pt(1)–S(2)	89.43(9)
4	Pt(1)–Pt(2)	2.6923(3)	Pt(1)–C(39)	2.011(5)
	Pt(1)–N(5)	2.065(5)	Pt(1)–N(1)	2.150(5)
	Pt(1)–S(2)	2.304(1)	Pt(1)–S(3)	2.484(1)
	Pt(2)–C(52)	2.015(6)	Pt(2)–N(6)	2.059(5)
	Pt(2)–N(2)	2.160(5)	Pt(2)–S(4)	2.309(1)
	Pt(2)–S(4)	2.466(1)	C(39)–Pt(1)–N(5)	81.7(2)
	C(39)–Pt(1)–N(1)	176.2(2)	N(5)–Pt(1)–N(1)	94.8(1)
	C(39)–Pt(1)–S(2)	95.1(1)	N(5)–Pt(1)–S(2)	175.4(1)
	N(1)–Pt(1)–S(2)	88.5(1)	C(39)–Pt(1)–S(3)	90.8(1)
	N(5)–Pt(1)–S(3)	91.4(1)	N(1)–Pt(1)–S(3)	90.6(1)
	S(2)–Pt(1)–S(3)	85.31(5)	C(52)–Pt(2)–N(6)	82.2(2)
	C(52)–Pt(2)–N(2)	177.7(2)	N(6)–Pt(2)–N(2)	95.7(1)
	C(52)–Pt(2)–S(1)	93.5(1)	N(6)–Pt(2)–S(1)	174.0(1)
	N(2)–Pt(2)–S(1)	88.7(1)	C(52)–Pt(2)–S(4)	91.1(1)
	N(6)–Pt(2)–S(4)	89.0(1)	N(2)–Pt(2)–S(4)	89.8(1)
	S(1)–Pt(2)–S(4)	86.83(5)		

κN,S)(pyt-κS)₂].[23] Upon entry of two NOS thiolate ligands at the axial ends of the dinuclear complexes, the resultant complexes **3** and **4** are formally Pt(III) with a distorted octahedral geometry. The most significant change is the Pt–Pt distances, which are reduced by *ca.* 10% to 2.685(1) Å and 2.6923(3) Å for **3** and **4**, respectively, due to the existence of the Pt–Pt bond.[20] These distances are similar to or slightly longer than those in the other related Pt^III–Pt^III complexes.[11,23–26,28] Again, comparing **4** with [Pt₂(bzq)₂(μ-NSS-κN,S)₂X₂] (Pt–Pt = 2.6420(3) Å for X = Cl, 2.6435(4) Å for X = Br and 2.6690(4) Å for X = I),[28] the difference in the Pt–Pt distances could be attributed to the stronger *trans* influence of the axial thiolate ligand, as was previously observed in [Pt₂(ppy)₂(μ-pyt-κN,S)₂(pyt-κS)₂] and [Pt₂(ppy)₂(μ-pyt-κN,S)₂Cl₂].[23,35]

The dihedral angles of cyclometalating ligands, ppy in **1** and **3** are 26.94° and 14.39°, respectively. From **2** to **4**, π–π separation of cyclometalating ligands (centroid to centroid distance) significantly decreases from 3.738 to 3.444 Å and the dihedral angle of the two cyclometalating ligands, bzq, changes from 6.81° to 5.89°, indicating an enhanced π–π interaction of the cyclometalating ligands in **4**.

Single crystals of **5** were obtained by slow diffusion of Et₂O into the CHCl₃ solution of **4**. X-ray diffraction analysis of **5** reveals that two axial NOS ligands are disordered due to the partial replacement by Cl⁻ from CHCl₃ (see ESI† for the detailed structure parameters of **5**). This suggests that ligand displacement could take place when another donor ligand is present in the system.

To gain a deeper understanding on the Pt–Pt interaction in the dinuclear Pt(II) and Pt(III) systems and their reactivities, density function theory (DFT) analysis was performed using **1** and **3** as models. The DFT optimized structures are in good agreement with the X-ray structures (see ESI†). There is no Pt–Pt bond formation in **1** as expected since the HOMO is the antibonding orbital between two Pt d_{z^2} orbitals (Fig. 3a). Adding an electron to **1** does not induce any obvious structural change, because it locates to the ring of the cyclometalating ligand. Therefore, the reduction is ligand-based rather than metal-based for **1**. Mulliken

3

4
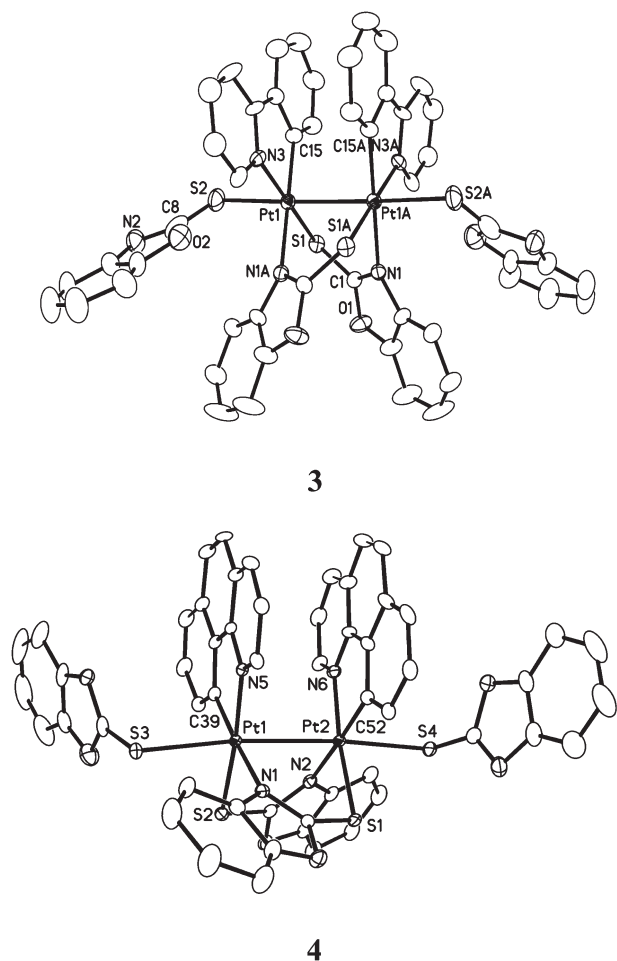
Fig. 2 ORTEP diagrams of **3** and **4** (30% probability ellipsoids). Solvent molecules and hydrogen atoms are omitted.


(a)   (b)
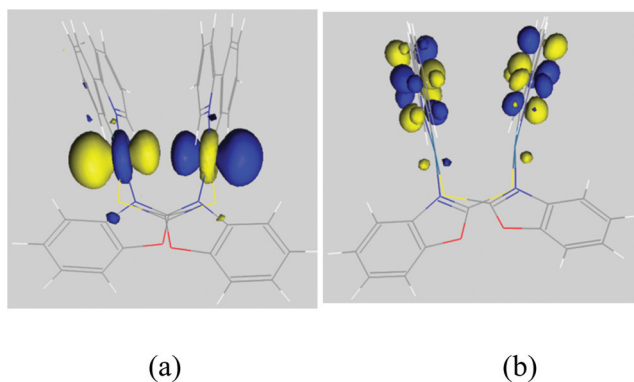
Fig. 3 (a) HOMO and (b) LUMO of **1**.

charge analysis suggests a Pt–Pt bonding interaction with overlap integral of 0.117 in **3**. The LUMO of **3** is the antibonding orbital between Pt centers and the axial NOS ligand (Fig. 4b). Adding an electron to this orbital will weaken both Pt–Pt and Pt–S bonds. The LUMO+1 of complex **3** is the antibonding orbital on the phenylpyridine ligand, which is very similar to the LUMO of **1** (Fig. 3b). The reduction product of **3** is hence structurally similar to **1** (see ESI†) as experimentally
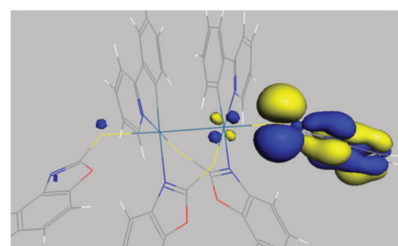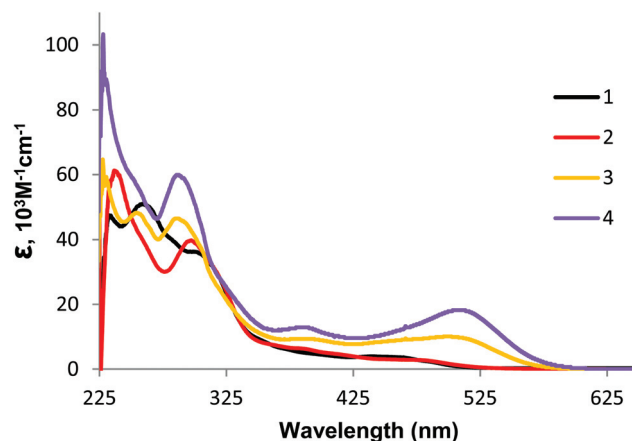

(a)
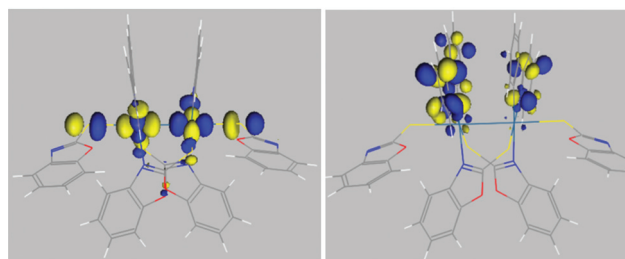
(b)   (c)

**Fig. 4** (a) HOMO, (b) LUMO and (c) LUMO+1 of **3**.

Fig. 5 UV-vis absorption spectra of **1**–**4** recorded in degassed CH_2Cl_2 at r.t.

evidenced in the reduction of Pt(III) to Pt(II) by $NaBH_4$ (*vide supra* and see also experimental part). However, complex **3** is theoretically hard to be oxidized since an electron cannot be easily removed from the terminal thiolate ligand ring. (Fig. 4c).

Photophysical studies

Absorption spectra. UV-vis absorption spectra of complexes **1**–**4** were recorded in degassed CH_2Cl_2 at r.t (Fig. 5). The high energy absorption bands with intense absorptions of **1**–**4** at $\lambda < 325$ nm are typically attributed to ligand-centered π–π* transitions.[11,28] The less intense, low energy bands of **1** and **2** between 350 and 500 nm can be assigned to MLCT and MMLCT.[11,28] For **3** and **4**, the low energy absorption bands occur in the region of 325–550 nm and can be originated from
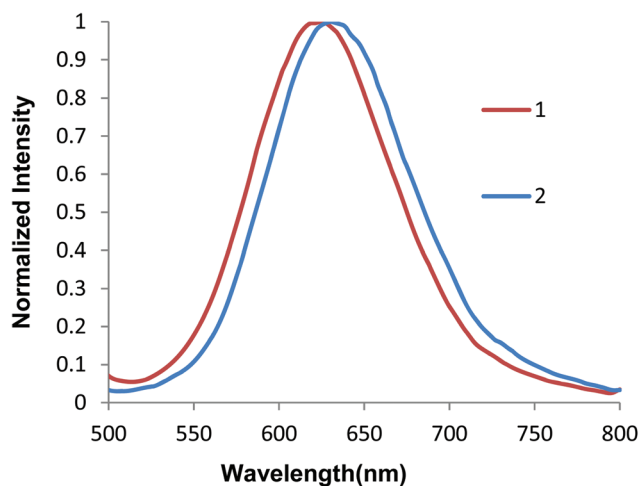
Fig. 6 Normalized luminescence spectra of **1** and **2** recorded in degassed CH_2Cl_2 solutions at r. t. Excitation wavelength, $\lambda_{ex} = 462$ nm.

Table 2 Photophysical data for **1** and **2** in degassed CH_2Cl_2 at r.t

Complex	PL (λ_{max}/nm)^a	Quantum yield (Φ)^b	τ^c/ns
1	625	0.0108	136
2	631	0.0095	153

^{a} $\lambda_{ex} = 462$ nm. ^{b} With respect to rhodamine 6G ($\Phi = 0.95$ in ethanol). ^{c} $\lambda_{ex} = 405$ nm.

Table 3 Cyclic voltammetric data for complexes **1–4**, [**1** + NOSH] and [**2** + NOSH]

Complex	Cyclic voltammetry		
	$E_{pa}[E_{pc}]$ (V)	ΔE_p (V)	$E_{1/2}$ (V)
1	0.896[0.705]	0.191	0.800
	1.158[0.816]	0.342	0.987
1 + NOSH	0.725[0.222]	0.503	0.474
	1.279[1.068]	0.211	1.174
2	0.916[0.715]	0.201	0.816
	1.188[0.866]	0.322	1.027
2 + NOSH	0.715[0.242]	0.473	0.478
	1.198[0.846]	0.352	1.022
3	0.322[−0.786]	1.108	−0.232
4	0.524[−0.745]	1.269	−0.110

Fig. 7 Cyclic voltammograms of **1** (0.6 mM) (solid line) and a mixture of **1** (0.6 mM) and NOSH (1.2 mM) (dashed line) in 0.05 M $^nBu_4NPF_6$ in CH_2Cl_2 at r.t. (scan rate = 50 mV s^{-1}, positive-potential scan direction).

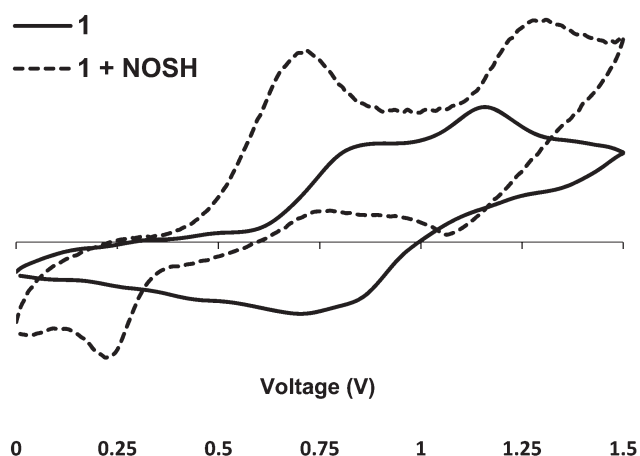an admixture of axial ligand-to-metal–metal charge transfer (XMMCT) transition and MC [dσ–dσ*] transitions.[24]

Emission spectra. Complexes **1** and **2** exhibit intense orange-red luminescence at 625 and 631 nm, respectively in CH_2Cl_2 at r.t. as shown in Fig. 6, which can be assigned to ^{3}MMLCT.[11,28,35] The slightly red-shifted emission of **2** is attributed to the lower lying π* orbital of the bzq ligand compared with the ppy ligand.[39] In general, **1** and **2** give blue-shifted emissions compared to the reported dinuclear Pt(II) complex, [Pt$_2$(ppy)$_2$(μ-pyt-κN,S)$_2$] (λ_{em} = 648 nm in EtOH–MeOH (4/1 v/v))[35] and [Pt$_2$(bzq)$_2$((μ-NSS-κN,S)$_2$] (λ_{em} = 665 nm in CH_2Cl_2).[28] The slightly longer intramolecular Pt^{II}–Pt^{II} separations in **1** and **2** may be responsible for blue-shifted emission due to the increased transition energy between dσ* and the ligand-based π* oribital.[17,18] Table 2 lists the photophysical data of **1** and **2**. Complexes **1** and **2** have higher quantum yields and longer lifetimes compared to [Pt$_2$(ppy)$_2$(μ-pyt-κN,S)$_2$] (Φ = 0.005; τ = 94 ns)[35] but lower quantum yield than [Pt$_2$(bzq)$_2$(μ-NSS-κN,S)$_2$] in solution (λ_{em} = 677 nm in toluene, Φ = 0.44; λ_{em} = 665 nm in CH_2Cl_2, Φ = 0.19) and solid state (λ_{em} = 648 nm, Φ = 0.62).[28] Complexes **3** and **4** are non-emissive in CH_2Cl_2 at r.t. in the visible range (up to 800 nm) as expected in d^7–d^7 complexes.[24]

Electrochemical studies

The electrochemical properties of **1–4** have been studied by cyclic voltammetry (CV) in CH_2Cl_2 with $^nBu_4NPF_6$ as

supporting electrolyte. Both **1** and **2** exhibit the electrochemically quasi-reversible oxidation process with E_{pa} = 0.896 and 1.158 V for **1** and 0.916 and 1.188 V for **2** (vs. Ag/AgCl/3 M KCl), corresponding to two steps of one-electron oxidation from Pt$^{II}_2$ to Pt$^{III}_2$ (Table 3 and Fig. 7 and 8). Complexes **1** and **2** are less susceptible to oxidation than [Pt$_2$(ppy)$_2$(μ-pyt-κN,S)$_2$] which has been reported to have an irreversible oxidation of Pt(II) to Pt(III) (E_{pa} = 0.58 V vs. NHE).[35] When the solution is doped with NOSH, a cathodic shift can be observed for the first one-electron oxidation wave with E_{pa} = 0.725 V for [**1** + NOSH] and 0.715 V for [**2** + NOSH], respectively (Table 3 and Fig. 7 and 8), suggesting that NOSH promotes this step of one-electron oxidation for both complexes. However, the second electron oxidation peak shows an anodic shift with E_{pa} = 1.279 V for [**1** + NOSH] and E_{pa} = 1.198 V for [**2** + NOSH]. It indicates that mixed-valent Pt(II)–Pt(III) species electrochemically produced in NOSH-doped solution are less susceptible to oxidation. The reduction waves (E_{pc}) of **3** and **4** appear at −0.786 and −0.745 V, respectively (the cathodic limit is −1 V) (Table 3 and Fig. 9).
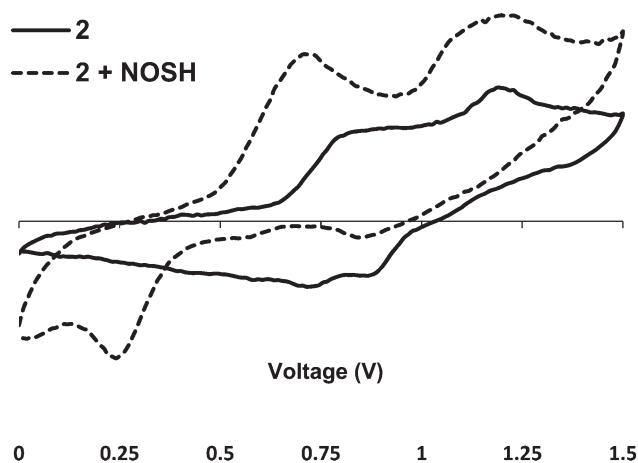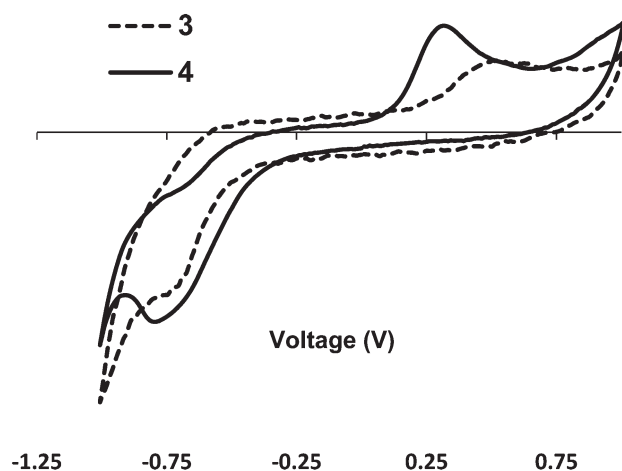
Fig. 8 Cyclic voltammograms of **2** (0.6 mM) (solid line) and a mixture of **2** (0.6 mM) and NOSH (1.2 mM) (dashed line) in 0.05 M $^{n}Bu_4NPF_6$ in CH_2Cl_2 at r.t. (scan rate = 50 mV s^{-1}, positive-potential scan direction).

Fig. 9 Cyclic voltammograms of **3** (0.6 mM) (dash line) and **4** (0.6 mM) (solid line) in 0.05 M $^{n}Bu_4NPF_6$ in CH_2Cl_2 at r.t. (scan rate = 50 mV s^{-1}, negative-potential scan direction).

Conclusion

We have demonstrated a photo- and electro-active dinuclear structural motif in which two square planar Pt(II) moieties can be juxtaposed by a combinative use of two sets of anionic ligands, bridging benzoxazole-2-thiolate and chelating 2-phenylpyridine and benzo[h]quinoline. The dinuclear core structure $Pt_2(C^\wedge N)_2$-$(S^\wedge N)_2$ ($C^\wedge N$ = ppy and bzq and $S^\wedge N$ = (μ-NOS-κN,S)$_2$ is sufficiently robust to withstand oxidation (metal-based). Yet, the bridging ligands are sufficiently flexible to allow the metals to come into bonding contacts upon oxidative entry of axial ligands. This form of redox-sensitive and reversible Pt–Pt bonding changes with preservation of the dinuclear core could provide a useful molecular sensing tool due to the different photoluminescent properties of Pt(II) and Pt(III) dinuclear complexes. The axial and equatorial approaches of the benzoxazole-2-thiolate ligands give rise to two different coordination modes, *viz.* bridging and terminal. This demonstrates the inherent flexibility of a hybrid ligand that is able to adapt to environmental changes. Such coordinative adaptability has prompted us to examine other structural forms that can be supported by these ligands.

Experimental

General procedures

All chemicals and solvents were used as purchased. The reactions were conducted under laboratory conditions without nitrogen protection. ^{1}H, ^{13}C NMR and ^{195}Pt spectra were recorded on a Bruker AMX 500 MHz FT NMR spectrometer. Na_2PtCl_6 in D_2O was used as standard reference for ^{195}Pt NMR. [Pt(L)-(μ-Cl)]$_2$ (L = ppy (2-phenylpyridine) or bzq (benzo[h]quinoline)) were synthesized according to the literature.[40] Elemental analyses for C, H, N and S were conducted on a Perkin-Elmer PE 2400 CHNS elemental analyzer. ESI-MS was performed on a Bruker amaZon X ion trap mass spectrometer or Thermo Finnigan LCQ spectrometer. Electrochemistry was performed on Metrohm AUTOLAB assembly with 3 electrode setup using 1.5 mm radius of glassy carbon as the working electrode, 3 M KCl, Ag/AgCl as the reference electrode and 0.8 × 0.7 cm of platinum blade as the counter electrode. UV-vis absorption spectra were recorded on a Shimadzu UV-1601 spectrophotometer. Emission spectra were measured using Perkin-Elmer LS55 Luminescence spectrofluorimeter. The lifetime measurement of the samples was recorded with Time-Correlated Single Photon Counting (TCSPC) Module and Picosecond Event Timer (PicoHarp 300). The samples were excited by the 405 nm line of a picosecond pulsed laser diode head (PicoQuant PDL 800-B). The photoluminescence was dispersed through a monochromator (Acton SpectroPro 2300i) and detected with a liquid N_2 cooled CCD camera (Princeton, Spec-10:100). Quantum yield analysis was using comparative method corresponding to rhodamine 6G as reference.[41]

Synthesis of 1 and 3

[Pt(L)(μ-Cl)]$_2$ (L = ppy (2-phenylpyridine)) (0.2 g, 0.26 mmol) was added to a THF solution (5 ml) of 2-mercaptobenzoxazole (0.165 g, 1.09 mmol) and NaOAc (0.18 g, 2.19 mmol). The suspension was stirred at r.t. overnight. The resultant dark red solution was vacuum dried, and the crude products were purified and separated by column chromatography by using hexane, CH_2Cl_2 and 10 : 1 of CH_2Cl_2–acetone as eluents to give complexes **1** and **3**. Complex **1** was obtained as a bright orange yellow solid, yield (0.09 g, 35%). Single crystal suitable for X-ray diffraction was grown by slow diffusion of Et_2O into CH_2Cl_2 sample solution. ^{1}H NMR (500 MHz, CD_2Cl_2): δ = 7.77–7.74 (m, 4H), 7.64 (d, J = 8.0 Hz, 2H) 7.50 (td, J = 7.5, 1.5 Hz, 2H), 7.37–7.35 (m, 2H), 7.22–7.19 (m, 4H), 7.15 (d, J = 8.0 Hz, 2H), 7.02–7.00 (d, J = 6.5 Hz, 2H), 6.81 (t, J = 7.5 Hz, 2H), 6.68–6.65 (m, 4H). ^{13}C NMR (125.77 MHz, CD_2Cl_2): δ = 175.49, 165.58, 151.61, 147.76, 144.41, 141.72, 139.25, 137.87, 133.96, 128.57, 123.62, 123.10, 122.61, 122.51, 121.40, 117.87, 115.47, 109.20. ^{195}Pt NMR (107.09 MHz, CD_2Cl_2): δ = −3728.58 ppm. Anal. Calcd for $C_{36}H_{24}N_4O_2Pt_2S_2$: C, 43.29; H, 2.42; N, 5.61;

S, 6.42. Found: C, 43.60; H, 2.42; N; 5.48; S, 6.42. ESI-MS (m/z, %, L = C_7H_4NOS): $[M - L]^+$ (848.01, 100); $[M + H]^+$ (999.06, 50).

Complex **3** was obtained as a red solid, yield (0.075 g, 23%). Single crystal suitable for X-ray diffraction was grown by slow diffusion of Et_2O into CH_2Cl_2 sample solution. ^1H NMR (500 MHz, CD_2Cl_2): $\delta = 8.52$–8.50 (m, 2H), 7.85 (d, $J = 5.5$ Hz, 2H), 7.53–7.51 (m, 2H), 7.33 (td, $J = 8$, 1.5 Hz, 2H), 7.29–7.27 (m, 4H), 7.12 (dd, $J = 7.5$, 1.0 Hz, 2H), 7.08–7.06 (m, 2H), 6.99 (dd, $J = 5.5$, 3.5 Hz, 4H), 6.84–6.81 (m, 4H), 6.68–6.66 (m, 2H), 6.53 (td, $J = 7.5$, 1.0 Hz, 2H), 6.48 (td, $J = 8.0$, 1.5 Hz, 2H), 6.42 (dd, $J = 7.5$, 1.5 Hz, 2H). ^{13}C NMR (125.77 MHz, CD_2Cl_2): $\delta = 181.55$, 166.19, 161.95, 152.89, 151.78, 147.54, 143.19, 141.17, 139.19, 138.40, 138.14, 130.71, 130.13, 124.78, 124.71, 124.03, 123.86, 123.44, 123.33, 123.09, 119.64, 119.28, 118.07, 110.49, 109.37. ^{195}Pt NMR (107.09 MHz, CD_2Cl_2): $\delta = -2542.24$ ppm. Anal. Calcd for $C_{51}H_{35}N_6O_4Pt_2S_4$: C, 46.61; H, 2.68; N, 6.39; S, 9.76. Found: C, 46.28; H, 2.57; N, 6.32; S, 9.68. ESI-MS (m/z, %, L = C_7H_4NOS): $[M - L]^+$ (1148.89, 100); $[M - 2L + e]^+$ (997.92, 60)

Synthesis of 2 and 4

Complexes **2** and **4** were prepared by a similar method as described for complexes **1** and **3**. $[Pt(L)(\mu-Cl)]_2$ (L = bzq (benzo[h]quinoline)) (0.2 g, 0.245 mmol) was used as a starting material. Complex **2** was obtained as an orange solid, yield (0.082 g, 32%). Single crystals suitable for X-ray diffraction were grown by slow diffusion of Et_2O into CH_2Cl_2 sample solution. ^1H NMR (500 MHz, CD_2Cl_2): $\delta = 7.83$ (dd, $J = 5.5$, 1.5 Hz, 2H), 7.75 (dd, $J = 7.0$, 1.5 Hz, 2H), 7.71–7.69 (m, 4H), 7.45 (dd, $J = 7.0$, 2.0 Hz, 2H), 7.27 (d, $J = 9.0$ Hz, 2H), 7.22 (qd, $J = 7.0$, 1.5 Hz, 4H), 7.11 (d, $J = 2.5$ Hz, 2H), 7.07 (d, $J = 8.5$ Hz, 2H), 6.98 (t, $J = 7.5$ Hz, 2H), 6.82 (q, $J = 8$, 5.5 Hz, 2H). ^{13}C NMR (125.77 MHz, CD_2Cl_2): $\delta = 175.96$, 154.03, 151.66, 146.92, 140.27, 139.44, 138.68, 136.43, 132.24, 130.71, 127.94, 127.79, 125.13, 123.67, 123.13, 122.12, 120.61, 119.88, 115.32, 109.26. ^{195}Pt NMR (107.09 MHz, CD_2Cl_2): $\delta = -3729.55$ ppm. Anal. Calcd for $C_{40}H_{24}N_4O_2Pt_2S_2$: C, 45.89; H, 2.31; N, 5.35; S, 6.13. Found: C, 45.53; H, 2.51; N; 5.16; S, 6.29. ESI-MS (m/z, %): $[M + Na]^+$ (1068.7, 100).

Complex **4** was obtained as a dark red solid, yield (0.056 g, 17%). Single crystals suitable for X-ray diffraction were grown by layering a CH_2Cl_2 sample solution with hexane. ^1H NMR (500 MHz, CD_2Cl_2): $\delta = 8.51$ (dd, $J = 8.0$, 1.0 Hz, 2H), 7.68 (d, $J = 1.5$ Hz, 2H), 7.61 (dd, $J = 5.5$, 1.5 Hz, 2H), 7.37–7.28 (m, 8H), 6.97 (t, $J = 7.5$ Hz, 2H), 6.91 (t, $J = 5.5$ Hz, 4H), 6.82–6.77 (m, 6H), 6.58 (dd, $J = 8.0$, 5.5 Hz, 2H), 6.46–6.44 (m, 2H). ^{13}C NMR (125.77 MHz, CD_2Cl_2): $\delta = 182.97$, 165.47, 153.19, 151.18, 149.64, 146.69, 142.50, 139.28, 136.77, 135.99, 135.41, 133.16, 129.71, 128.27, 127.96, 126.22, 124.82, 124.76, 123.51, 123.23, 123.03, 122.98, 121.01, 119.09, 117.95 110.76, 109.16. ^{195}Pt NMR (107.09 MHz, CD_2Cl_2): $\delta = -2548.29$ ppm. Anal. Calcd for $C_{54}H_{32}N_6O_4Pt_2S_4$: C, 48.14; H, 2.39; N, 6.24; S, 9.52. Found: C, 48.36; H, 2.54; N, 6.19; S, 9.65. ESI-MS (m/z, %, L = C_7H_4NOS): $[M - L]^+$ (1196.87, 100); $[M - 2L + e]^+$ (1046.06, 80).

Reduction of 3 and 4

A mixture of complex **3** (20 mg, 0.016 mmol) or **4** (22 mg, 0.016 mmol) with $NaBH_4$ (6 mg, 0.16 mmol) was stirred in THF (5 ml) at r.t. overnight. After removing the solvent, the crude products were separated and purified by column chromatography. Formation of complex **1** and **2** was confirmed by ^1H NMR and ESI-MS. Yields: **1**, 8 mg (51%); **2**, 9 mg (54%).

Oxidation of 1 and 2

A mixture of complex **1** (30 mg, 0.03 mmol) or **2** (32 mg, 0.03 mmol) with 2-mercaptobenzoxazole (10 mg, 0.066 mmol) and (11 mg, 1.32 mmol) was stirred in THF (5 ml) at r.t. overnight. The resultant solution was vacuum dried, and the crude products were purified and separated by column chromatography. Formation of complexes **3** and **4** was confirmed by ^1H NMR and ESI-MS. Yields: **1**, 12 mg (30%); **2**, 10 mg (25%).

X-ray crystallography

Diffraction measurements were conducted at 100(2)–223(2) K on a Bruker AXS APEX CCD diffractometer by using Mo Kα radiation ($\lambda = 0.71073$ Å). The data were corrected for Lorentz and polarization effects with the SMART suite of programs and for absorption effects with SADABS.[42] Structure solutions and refinements were performed by using the programs SHELXS-97[43] and SHELXL-97.[44] The crystal of **4·3CH₂Cl₂** is monoclinic, space group $P2_1/n$. The asymmetric unit contains one molecule of the compound $C_{54}H_{32}N_6O_4S_4Pt_2$ and three CH_2Cl_2 solvate molecules that are disordered. They were refined in two groups of occupancy ratio 66 : 34. There were two large residual peaks (heights over 6.0 e) which could not be accounted for. This is interpreted as a small percentage of disordered complex (about 2.5%), because the distance of their two peaks was the same as the Pt–Pt distance. Other residual peaks of this disordered complex did not appear because the peak heights would be too low. Refinement with this scheme reduced the R values to a very low level. Final R values are $R_1 = 0.0395$ and w$R_2 = 0.1032$ for 2-theta up to 55°. The crystal of **5·CHCl₃** is monoclinic, space group $P2_1/n$. The asymmetric unit contains one molecule of the compound $C_{54}H_{32}N_6O_4S_4Pt_2$ and one $CHCl_3$. Initial refinement results showed that the two axial S-containing ligand anions were disordered. The disorder appeared to be due to partial replacement by $CHCl_3·Cl$, where the $CHCl_3$ is needed for space filling purposes. Free variable refinement indicated about 22% being replaced. Final refinement with this scheme resulted in very good R values with $R_1 = 0.0379$ and w$R_2 = 0.089$. Selected crystal data for complexes **1–5** are summarized in Table 4.

Calculation details

All DFT calculations were performed using the SIESTA package[45] with numerical atomic orbital basis sets and Troullier–Martins norm-conserving pseudopotentials.[46] The exchange-correlation functional utilized was GGA-PBE,[47] and the optimized double-ζ plus polarization (DZP) basis set was employed.

Table 4 Crystallographic data for complexes **1–5**

Complex	$1 \cdot CH_2Cl_2$	2	3	$4 \cdot 3CH_2Cl_2$	$5 \cdot CHCl_3$
Formula	$C_{37}H_{26}Cl_2N_4O_2Pt_2S_2$	$C_{40}H_{24}N_4O_2Pt_2S_2$	$C_{50}H_{32}N_6O_4Pt_2S_4$	$C_{57}H_{38}Cl_6N_6O_4Pt_2 S_4$	$C_{52.25}H_{31.75}Cl_{4.75}N_{5.50}O_{3.50}Pt_2S_{3.50}$
M_W	1083.82	1046.93	1299.24	1602.05	1463.36
T/K	100(2)	223(2)	223(2)	100(2)	223(2)
Cryst. syst.	Triclinic	Monoclinic	Monoclinic	Monoclinic	Monoclinic
Space group	$P\bar{1}$	$P2_1/C$	$C2/c$	$P2_1/n$	$P2_1/c$
a/Å	11.0333(13)	22.816(7)	17.731(5)	14.2649(9)	15.2972(11)
b/Å	11.1183(13)	10.769(4)	17.059(5)	18.2230(12)	14.0052(10)
c/Å	15.4788(19)	13.587(4)	15.670(5)	21.3226(14)	22.8163(17)
α/°	97.666(2)	90	90	90	90
β/°	105.770(2)	98.587(7)	109.995(6)	95.1340(10)	92.0850(10)
γ/°	109.916(2)	90	90	90	90
V/Å^3	1663.6(3)	3301.0(18)	4454(2)	5520.6(6)	4884.9(6)
Z	2	4	4	4	4
D_{calc}/g cm^{-3}	2.164	2.107	1.937	1.928	1.990
Reflections collected	22142	21755	14814	39123	34500
R_{int}	0.0308	0.0770	0.0558	0.0342	0.0492
Parameters	442	451	298	737	662
GOF	1.042	0.994	1.103	1.054	1.033
R_1 [$I > 2\sigma(I)$]	0.0215	0.0506	0.055	0.0395	0.0379
wR_2 [$I > 2\sigma(I)$]	0.0501	0.0971	0.1304	0.1032	0.089

Acknowledgements

References

1 F. A. Cotton, L. R. Falvello and S. Han, *Inorg. Chem.*, 1982, **21**, 2889–2891.

2 K. Umakoshi, I. Kinoshita, A. Ichimura and S. Ooi, *Inorg. Chem.*, 1987, **26**, 3551–3556.

3 K. Umakoshi and Y. Sasaki, *Inorg. Chem.*, 1997, **36**, 4296–4297.

4 K. Umakoshi, I. Kinoshita, Y. Fukuiyasuba, K. Matsumoto, S. Ooi, H. Nakai and M. Shiro, *J. Chem. Soc., Dalton Trans.*, 1989, 815–819.

5 H. Kunkely and A. Vogler, *J. Am. Chem. Soc.*, 1990, **112**, 5625–5627.

6 C. W. Chan, T. F. Lai, C. M. Che and S. M. Peng, *J. Am. Chem. Soc.*, 1993, **115**, 11245–11253.

7 V. M. Miskowski, V. H. Houlding, C. M. Che and Y. Wang, *Inorg. Chem.*, 1993, **32**, 2518–2524.

8 S. D. Cummings and R. Eisenberg, *J. Am. Chem. Soc.*, 1996, **118**, 1949–1960.

9 B. C. Tzeng, W. F. Fu, C. M. Che, H. Y. Chao, K. K. Cheung and S. M. Peng, *J. Chem. Soc., Dalton Trans.*, 1999, 1017–1023.

10 O. Asada, K. Umakoshi, K. Tsuge, S. Yabuuchi, Y. Sasaki and M. Onishi, *Bull. Chem. Soc. Jpn.*, 2003, **76**, 549–555.

11 R. Aoki, A. Kobayashi, H.-C. Chang and M. Kato, *Bull. Chem. Soc. Jpn.*, 2011, **84**, 218–225.

12 M. Kato, *Bull. Chem. Soc. Jpn.*, 2007, **80**, 287–294.

13 K. M. C. Wong and V. W. W. Yam, *Coord. Chem. Rev.*, 2007, **251**, 2477–2488.

14 B. Ma, P. I. Djurovich, S. Garon, B. Alleyne and M. E. Thompson, *Adv. Funct. Mater.*, 2006, **16**, 2438–2446.

15 X. G. Wu, Y. Liu, Y. F. Wang, L. Wang, H. Tan, M. X. Zhu, W. G. Zhu and Y. Cao, *Org. Electron.*, 2012, **13**, 932–937.

16 K. Saito, Y. Hamada, H. Takahashi, T. Koshiyama and M. Kato, *Jpn. J. Appl. Phys.*, 2005, **44**, L500–L501.

17 B. W. Ma, J. Li, P. I. Djurovich, M. Yousufuddin, R. Bau and M. E. Thompson, *J. Am. Chem. Soc.*, 2005, **127**, 28–29.

18 M. Kato, A. Omura, A. Toshikawa, S. Kishi and Y. Sugimoto, *Angew. Chem., Int. Ed.*, 2002, **41**, 3183–3185.

19 B.-C. Tzeng, T.-H. Chiu, S.-Y. Lin, C.-M. Yang, T.-Y. Chang, C.-H. Huang, A. H.-H. Chang and G.-H. Leo, *Cryst. Growth Des.*, 2009, **9**, 5356–5362.

20 D. M. Roundhill, H. B. Gray and C. M. Che, *Acc. Chem. Res.*, 1989, **22**, 55–61.

21 T. G. Appleton, K. A. Byriel, J. M. Garrett, J. R. Hall, C. H. L. Kennard, M. T. Mathieson and R. Stranger, *Inorg. Chem.*, 1995, **34**, 5646–5655.

22 A. R. Dick, J. W. Kampf and M. S. Sanford, *Organometallics*, 2005, **24**, 482–485.

23 T. Koshiyama and M. Kato, *Acta Crystallogr.*, 2005, **61**, M173–M176.

24 M. A. Bennett, S. K. Bhargava, E. C.-C. Cheng, W. H. Lam, T. K.-M. Lee, S. H. Privér, J. R. Wagler, A. C. Willis and V. W.-W. Yam, *J. Am. Chem. Soc.*, 2010, **132**, 7094–7103.

25 C. M. Che, F. H. Herbstein, W. P. Schaefer, R. E. Marsh and H. B. Gray, *J. Am. Chem. Soc.*, 1983, **105**, 4604–4607.

26 K. A. Alexander, S. A. Bryan, F. R. Fronczek, W. C. Fultz, A. L. Rheingold, D. M. Roundhill, P. Stein and S. F. Watkins, *Inorg. Chem.*, 1985, **24**, 2803–2808.

27 A. E. Stiegman, V. M. Miskowski and H. B. Gray, *J. Am. Chem. Soc.*, 1986, **108**, 2781–2782.

28 V. Sicilia, J. Forniés, J. M. Casas, A. Martín, J. A. López, C. Larraz, P. Borja, C. Ovejero, D. Tordera and H. Bolink, *Inorg. Chem.*, 2012, **51**, 3427–3435.

29 J. Li, L. L. Koh and T. S. A. Hor, *Chem. Commun.*, 2009, 3416–3418.

30 J. Li, F. Li, L. L. Koh and T. S. A. Hor, *Dalton Trans.*, 2010, **39**, 2441–2448.

31 J. Li and T. S. A. Hor, *Dalton Trans.*, 2008, 6619–6623.

32 J. J. Hu, S.-Q. Bai, H. H. Yeh, D. J. Young, Y. Chi and T. S. A. Hor, *Dalton Trans.*, 2011, **40**, 4402–4406.

33 W.-H. Zhang, J. J. Hu, D. J. Young and T. S. A. Hor, *Organometallics*, 2011, **30**, 2137–2143.

34 W.-H. Zhang, X.-H. Zhang, A. L. Tan, M. A. Yong, D. J. Young and T. S. A. Hor, *Organometallics*, 2012, **31**, 553–559.

35 T. Koshiyama, A. Omura and M. Kato, *Chem. Lett.*, 2004, **33**, 1386–1387.

36 N. Marino, C. H. Fazen, J. D. Blakemore, C. D. Incarvito, N. Hazari and R. P. Doyle, *Inorg. Chem.*, 2011, **50**, 2507–2520.

37 F. Liu, W. Chen and D. Wang, *Dalton Trans.*, 2006, 3445–3453.

38 W. Chen and K. Matsumoto, *Inorg. Chim. Acta*, 2003, **342**, 88–96.

39 Y. Chi and P.-T. Chou, *Chem. Soc. Rev.*, 2010, **39**, 638–655.

40 N. Godbert, T. Pugliese, I. Aiello, A. Bellusci, A. Crispini and M. Ghedini, *Eur. J. Inorg. Chem.*, 2007, 5105–5111.

41 R. F. Kubin and A. N. Fletcher, *J. Lumin.*, 1982, **27**, 455–462.

42 *SADABS: Area-Detection Absorption Correction*, Bruker AXS Inc., Madison, WI, 1995.

43 G. M. Sheldrick, *SHELXS-97 Program for Crystal Structure Solution*, University of Göttingen, Göttingen, Germany, 1997.

44 G. M. Sheldrick, *SHELXL-97 Program for Crystal Structure Refinement*, University of Göttingen, Göttingen, Germany, 1997.

45 J. M. Soler, E. Artacho, J. D. Gale, A. Garcia, J. Junquera, P. Ordejon and D. Sanchez-Portal, *J. Phys.: Condens. Matter*, 2002, **14**, 2745–2779.

46 N. Troullier and J. L. Martins, *Phys. Rev. B: Condens. Matter*, 1991, **43**, 1993–2006.

47 J. P. Perdew, K. Burke and M. Ernzerhof, *Phys. Rev. Lett.*, 1996, **77**, 3865–3868.